

08 AUG 03

Blending the Impulse Approximation with rational improvements for the double-differential Compton X-ray scattering cross section and with the Incoherent Approximation

Corneliu I. Costescu*

*Radiation Physics Division, Department of Radiation Oncology, Washington University in St. Louis, Campus Box 8224, 4921 Parkview, Place, St. Louis, MO 63110, USA

Jeffrey F. Williamson†

† Department of Radiation Oncology, Virginia Commonwealth University, 401 College Street, B-129, PO Box 980058, Richmond, VA 23298, USA

Iwan Kawrakow‡

‡ Ionizing Radiation Standards Division, National Research Council of Canada, Ottawa, K1A 0R6, Canada

(Dated: July 15, 2003)

A review of the Impulse Approximation (IA) for calculating Compton photon scattering probabilities by bound electrons reveals a paucity of measured, double-differential cross-section (DDCS) data with respect to angle and energy, especially for scattered photon with energies near that of the incident photon energy E . The K-shell DDCSs derived from IA display undesirable discontinuities and poorly match available experimental continuous DDCSs between the Compton energy E_c^0 and E . Similar discrepancies with respect to experiment are displayed by the S-matrix results. Because numerical evaluation of IA is so practical and straightforward, we have replaced the electron momentum in the energy-momentum conservation with an ad hoc concept of partial electron momentum to show the feasibility of reducing such discrepancies. In the proposed ad hoc DDCS, called here the blended impulse approximation (BIA), this replacement is combined with the incoherent approximation. BIA removes the undesirable discontinuities in the DDCS, indicates better agreement with existing experimental data, and provides a general DDCS form for incorporating evaluated experimental data. We suggest that the S-matrix energy-momentum conservation could also use the ad hoc concept of partial electron momentum, for benefits similar to the IA case. Further development of BIA requires a measurement of a comprehensive set of DDCSs to help finding an adequate set of shell-dependent expressions for the partial electron momentum. In conclusion we suggest that the concept of partial electron momentum may have a direct physical significance for the photon: the Compton interaction is such that the photon sees only a part of the electron momentum. Alternatively, it might indicate the need for a reviewed mechanism of the Compton effect, different for free and bound electrons.

PACS numbers: 32.80.Cy

I. INTRODUCTION

The experimental and theoretical studies of X-ray energy loss through scattering by atomic electrons have a rich history [1, 2, 3, 4, 5, 6] beginning before Compton's pioneering work. These studies have continued to be an active area of research to the present day.

Measurement and theory indicate that the average scattered photon energy decreases as the scattering angle increases from 0 to π . At any given scattering angle θ , the energy distribution of the scattered photons is not singular but takes the form of an asymmetric continuous distribution around the Compton energy E_c^0 given by

$$E_c^0 = \frac{E}{1 + E(1 - \cos \theta)}, \quad (1)$$

where E is the energy of the incident photon measured in units of electron rest energy (mc^2). This distribution is described by the double-differential cross section (DDCS) versus the energy and solid angle of the emergent photon. Experiments and theory indicate that the width of this distribution decreases as the scattering angle approaches zero and as the target atomic number Z decreases. Experimental data that characterize these distributions are scarce, especially for scattered photon with energies near that of the incident photon energy E . Higher resolution measurements and the advent of high-intensity monoenergetic synchrotron beams may improve the experimental characterization of Compton scattering in the near future.

There are three basic theoretical approaches to the modeling of Compton scattering: the incoherent scattering function (ISF) or the generalized form factor (GFF) approach, the impulse approximation (IA), and the S-matrix theory. GFF [3,7] modifies the free-electron KN cross section by the incoherent scattering factor, which is derived from a model of the bound electron wave functions. The ISF attempts to correct for the reduced probability of scattering when the momentum transfer is small (forward directions or low-energy incident photons). The resultant single differential cross section (SDCS), which depends only on scattering angle, is widely used in dosimetry and radiation transport calculations. IA generalizes [8] the Klein-Nishina cross section to the case where the target electron is in motion according to its momentum distribution within the atom. The target electron is still treated as a free electron, but with a momentum distribution derived from the bound electron wave function. The IA assumes that the interaction is impulsive, i.e., it instantaneously transfers a large momentum, so that its potential energy does not change during the interaction, and the electron can leave the atom. This condition is not satisfied for small momentum transfers (weak impacts) occurring either when the incident photon energy E is small or when E is large but the scattering angle is small. However, IA leads [8] to approximate DDCSs that are very useful [9] in the calculation of fluence spectra at larger scattering angles (with no discontinuities).

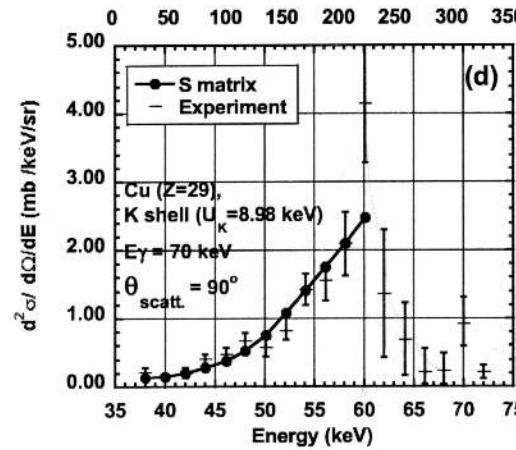
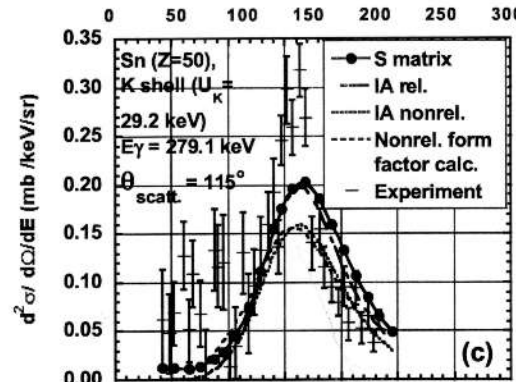
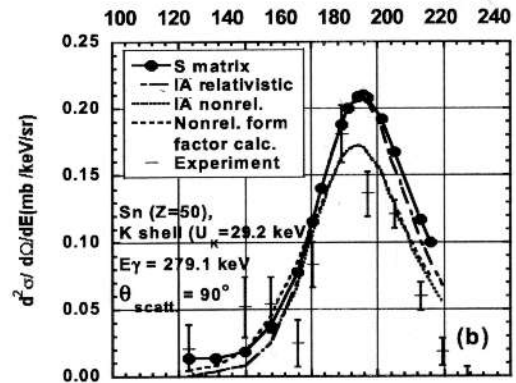
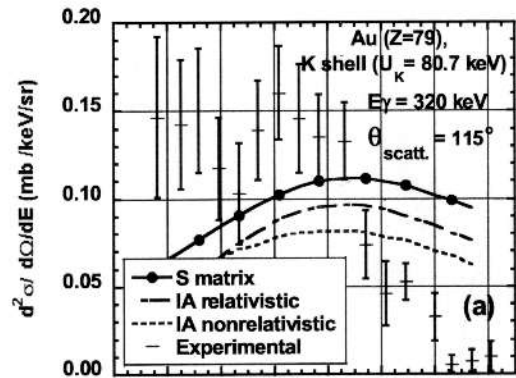
Applying energy and momentum conservation to the IA treatment of photon scattering by moving electrons allows, in principle, the final scattered photon energy E' to exceed $E - U_i$ and E , where U_i is the binding energy for the i -th shell. Such photons are not observed experimentally. To exclude such events, the Compton effect is restricted to those photon-atom collisions in which an electron is ejected from the atom in correlation with the emergent (scattered) photon. Thus, $E' > E - U_i$ is not allowed. This energy cut gives rise to a discontinuity at $E - U_i$.

Available experimental data suggests that the IA DDSCS does not correctly describe the scattered photon spectrum as E_c^0 approaches $E-U_i$. Figure 1(a) [10,11] shows significant and typical deviations of the calculated K-shell IA scattering distribution from measured results in the interval $(E_c^0, E-U_K)$. The measured scattering probability continuously decreases to zero as E' approaches $E-U_K$, in contrast with IA predictions. Figures 1(b) and 1(c) [10,12] illustrate the same trend. However, here the differences are less dramatic since the Compton profile is less broad than in Fig. 1(a). In both cases, IA energy spectra exhibit an unphysical discontinuity at $E-U_K$. The experimental spectrum shown by Fig. 1(d) [10,13] reveals scattered photons exceeding significantly the $E-U_K$ threshold while the calculated curve discontinuously falls to zero at this energy. Here, the Compton energy, $E_c^0 = 61.5$ keV is much closer to $E-U_K = 61.02$ keV, in contrast to Figures 1(a) - 1(c) (E_c^0 of 169.2, 180.51 and 157.06 keV respectively). Figures 1(a)-1(c) also show that S-matrix DDSCSs, derived from the original published figures, exhibit a similar pattern of discontinuities at $E-U_K$ and deviations from measurements.

Restricting IA to collisions in which the target electron is ejected, leads to discontinuities in the total DDSCS, as illustrated by our calculations for Cu in Figures 2(a) and 2(b). If the experimental curves from Figures 1 are true then the all-shell restricted DDSCSs from Fig. 2 have an implausible shape suggesting the need for further experimental and theoretical investigation. This conclusion is not necessarily in contradiction with the discontinuous all-shell DDSCSs reported in Ref. [14] for Pb, Sn and Cu for photons of 279.1 and 661.7 keV. Indeed, the 279.1 keV DDSCSs display a relatively smooth decrease around $E-U_i$ that can be reconciled with the experimental trend identified above from Fig. 1. In the higher energy case of 661.7 keV, the DDSCSs may have sharper discontinuities. However, in this case the DDSCSs are presented on a broad energy scale that may enhance the impression that there is a sharp cut in the DDSCS. Hence, at least for lower photon energies, we conclude that there is a clear discrepancy between the experimental and theoretical DDSCSs in the range $(E_c^0, E-U_i)$, and that there is a need for a consistent set of experimental DDSCSs showing the details of the spectrum around the energies $E-U_i$.

To our knowledge, the above discrepancies between theoretical and experimental characterizations of bound Compton scattering have not been previously recognized in the literature as indicating a major need to improve theoretical modeling of this phenomenon. The purpose of our paper is to propose ad hoc modifications of the current IA and GFF treatments of Compton scattering resulting in an improved DDSC in the energy interval $(E_c^0, E-U_i)$. The two central modifications are as follows. a) Use modified energy and momentum conservation conditions, equivalent to assuming that only a part of the momentum of the moving electron is observed by the incident photon. b) Include the ISF in the modified DDSCS such that its integral over solid angles and scattered energies yields a total cross section, is numerically equal to that derived from the GFF approach. Therefore, the proposed procedure incorporates electron-binding corrections as well as the IA electron momentum distributions. We call this approach the blended impulse approximation (BIA)

FIG. 1. Double differential cross section for photons scattered by electrons. a) $E = 320$ keV scattered on Au, K-shell, derived from Fig. 30(c) of Ref. 10 and Fig. 3 of Ref. 11; b) $E=279.1$ keV scattered on Sn, K-shell, derived from Fig. 30(a) Ref. 10 and Fig. 8 of Ref. 12; c) $E=279.1$ keV scattered on Sn, K-shell, derived from Fig. 30(b) of Ref. 10 and Fig. 9 of Ref. 12; d) $E = 70$ keV scattered on Cu, K-shell, derived from Fig. 32 of Ref. 10 and Fig. 2 of Ref. 13.



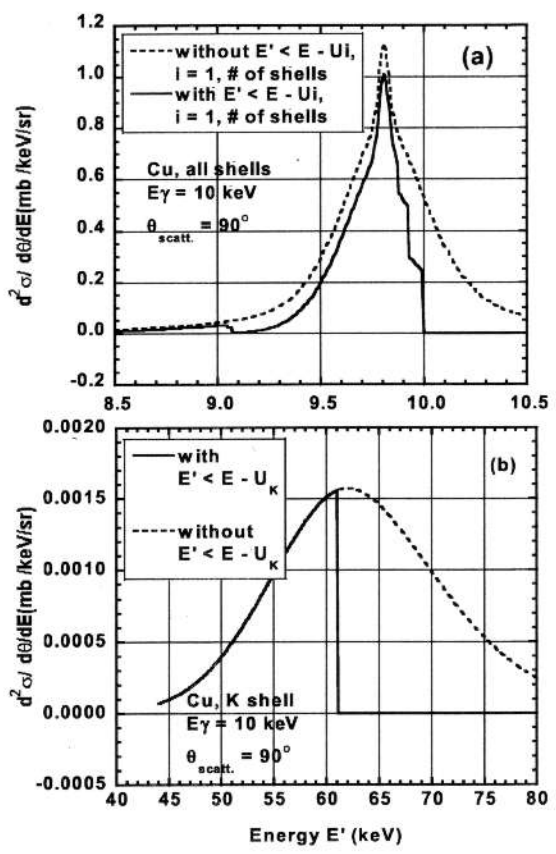


FIG. 2. Comparison of the IA-DDCS for Cu, with and without the QM restrictions $E' < E - U_i$. a) Photon energy = 10 keV, scattering angle of 90 degrees and $i = 1$, # of shells, and b) Photon energy = 70 keV, a scattering angle of 90 degrees, and $i = \text{shell K}$.

II. INCOHERENT SCATTERING (IS) and IMPULSE APPROXIMATION (IA) APPROACHES TO ELECTRON-BINDING EFFECTS

A. The ISF approximation

The generalized form factor (GFF) approach describes Compton scattering by the following single-differential cross section (SDCS):

$$\left[\frac{d\sigma}{d\cos\theta} \right]_{ISF} = \frac{d\sigma_{KN}}{d\cos\theta} S_{ISF}(E, \theta, Z). \quad (2)$$

Here, σ_{KN} is the Klein-Nishina (KN) cross section [15, 16], S_{ISF} is the incoherent scattering function [3,17], E is the incident photon energy, θ is the polar angle of the emergent photon, and Z is the atomic number of the interacting atom. The KN cross section is given by

$$\frac{d\sigma_{KN}}{d\cos\theta} = \pi r_0^2 \left(\frac{E}{E_c} \right)^2 X_{KN}, \quad X_{KN} = \left(\frac{E_c^0}{E} + \frac{E}{E_c} - \sin^2\theta \right), \quad (2a)$$

where $r_0 = e^2/(mc^2) = 2.8179380 \cdot 10^{-15}$ m is the classical electron radius. S_{ISF} is given by [3]

$$S_{ISF}(\vec{q}, Z) = \sum_{\epsilon > 0} |F_\epsilon(\vec{q}, Z)|^2 \quad (2b)$$

with

$$F_\epsilon(\vec{q}, Z) = \left\langle \Psi_\epsilon \left| \sum_{j=1}^Z \exp(i\vec{q} \cdot \vec{r}_j) \right| \Psi_0 \right\rangle, \quad (2c)$$

Here, Ψ_0 is the ground state wave function of the atom, Ψ_ϵ is the wave function for a stationary excited (or ionized) state of energy ϵ measured from the ground state, $\hbar \vec{q} = \vec{p}' - \vec{p} = \Delta\vec{p}$ (q is in units of $1/\text{length}$), where $\hbar = h/2\pi$; h = Planck's constant; \vec{p} and \vec{p}' are, respectively, the initial and the final momentum of the photon; and \vec{r}_n is the position of the n -th electron in an atom with Z electrons. In the forward direction, there is no energy transfer by inelastic scattering and hence no excitation or ionization. Thus, $\Psi_\epsilon \approx \Psi_0$ and $F_\epsilon(\vec{q}, Z)$ approaches the classical form factor $F(\vec{q}, Z)$ for elastic scattering. However, S_{ISF} approaches zero in this case due to the $\epsilon > 0$ restriction.

ISF neglects the Compton broadening effect and specifies a single emergent photon energy for each θ , rather than a spectrum. Practical ISF computation assumes that electronic excitation energies are small relative to E . The momentum transfer calculations assume that the incident and scattered photon energies are equal. Finally, Eq. (2c) sums up all final states even when the corresponding transitions are not allowed. However, S_{ISF} has two important practical properties: a) it approaches zero as θ (and hence, $|\vec{q}|$) goes to zero, and b) it approaches zero as E (and hence, $|\vec{q}|$) goes to zero. In other words, S_{ISF} is zero for scattering angles for momentum transfers of zero. These properties are consistent with the experimental data despite the approximate nature of the ISF derivation [17]

B. Impulse approximation

IA expands upon the simpler KN treatment of inelastic scattering by modeling effects due to motion of the target electrons. The practical result of IA is a DDCS with respect to the final photon energy and solid angle.

1. Energy and momentum conservation

The first step in deriving IA is to solve the relativistic energy and momentum conservation (EMC) relations for photon scattering on a bound electron as a two-body elastic collision. For a collision that occurs in a space specified by the vectors \vec{r} and \vec{r}' (see Fig. 3), in an electron potential energy V , the EMC relations are

$$\vec{p} + \vec{p}_e = \vec{p}' + \vec{p}'_e \quad (3a)$$

$$E + E_e + V(\vec{r}) = E' + E'_e + V(\vec{r}') \quad (3b)$$

$$E_e = \sqrt{1 + \vec{p}_e^2} \quad (3c)$$

$$E = p \quad (3d)$$

Here \vec{p} stands for momentum in units of mc , while E stands for energy in units of mc^2 and the unprimed and primed quantities describe the incident and scattered particle states, respectively. The momentum and energy of electron and photon states are denoted by the subscripted (by e) and un-subscripted quantities, respectively. As the collision is assumed to occur without appreciable change in position, then $\vec{r}' = \vec{r}$ and V drops out of Eq. (3b). The system (3) with no V describes the free electron at large distance from the atom (the observed electron) after the interaction with the photon, only if the effect of the potential V after the collision is small.

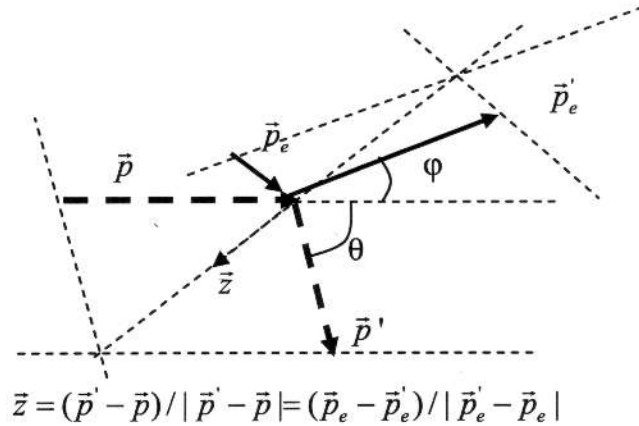


FIG. 3. The momentum conservation diagram for the collision of a photon with an electron. A useful choice of the z-axis is illustrated (in the direction of momentum transfer).

The equation system (3) is valid only for scattering angles $\theta > 0$. When $\theta = 0$, the EMC system is different since the energy and momentum magnitude of the photon and electron remain unchanged after collision. Hence, one must exercise caution in taking the limit $\theta \rightarrow 0$ to solutions of (3).

Both exact and approximate solutions can be derived from Eqs (3). Assuming a stationary electron ($p_e = 0$) leads to equation (1). Using approximate but still relativistic forms of Eqs. (3c) and (3d), a common implementation of IA[8] derives a one-to-one correspondence between the z-axis projection of \vec{p}'_e and E' . A similar correspondence can be derived when using electron energy from classical mechanics (nonrelativistic), by assuming E' is close to E . The common IA approximation presented next, while the exact solution is presented in the section on BIA.

The z-axis is chosen (Fig. 3) to denote the direction of the momentum transfer $\Delta \vec{p} = \hbar \vec{q} = \vec{p}' - \vec{p}$. Specifically, $\vec{p}' - \vec{p} = |\vec{p}' - \vec{p}| \hat{z}$, $\vec{p}'_e - \vec{p}_e = -(\vec{p}' - \vec{p}) = -|\vec{p}' - \vec{p}| \hat{z}$, $p_x = p'_x$, $p_y = p'_y$, $p_{e,x} = p'_{e,x}$, and $p_{e,y} = p'_{e,y}$. The first two equations can also be written as $p'_z - p_z = \Delta p$, and $p'_{e,z} - p_{e,z} = -\Delta p$ where $\Delta p = |\vec{p}' - \vec{p}| = \sqrt{|\vec{p}|^2 + |\vec{p}'|^2 - 2|\vec{p}||\vec{p}'|\cos\theta} = \sqrt{E^2 + E'^2 - 2EE'\cos\theta}$.

Hence,

$$\begin{aligned} E_e'^2 &= (E - E' + E_e)^2, \\ p'_{e,z} - p_{e,z} &= -\Delta p. \end{aligned} \tag{3e}$$

Or,

$$\begin{aligned} p_{z,e}^2 &= (E - E')^2 + 2(E - E')\sqrt{1 + \vec{p}^2} + p_{z,e}^2, \\ p'_{e,z} - p_{e,z} &= -\Delta p. \end{aligned} \quad (3f)$$

Assuming that $\sqrt{1 + \vec{p}^2} \approx 1$ in Eqs. (3f) leads to

$$p_{e,z}(E, \cos \theta, E') = \frac{EE'(1 - \cos \theta) + E' - E}{\Delta p}. \quad (4a)$$

Solving for E' , we obtain,

$$E'(E, \cos \theta, p_{e,z}) = \frac{E_c^0}{1 - p_{e,z}^2 \epsilon^2} \left[1 - p_{e,z}^2 \epsilon \cos \theta + p_{e,z} \sqrt{1 - 2\epsilon \cos \theta + \epsilon^2 (1 - p_{e,z}^2 \sin^2 \theta)} \right], \quad (4b)$$

where $\epsilon = E^0/E$. Equation (4a) can be written as

$$\frac{1}{E'} - \frac{1}{E} = (1 - \cos \theta) - \Delta p \cdot \frac{p_{e,z}}{EE'} \quad (4c)$$

The last term of (4c) leads to the Doppler-like broadening of the scattered photon energy spectrum since $p_{e,z}$ changes from one scattering event to another. Setting $p_{e,z} = 0$ implies that $E' = E_c^0$. Hence, the Compton peak is associated with $p_{e,z} = 0$ (scattering on electrons at rest). It follows that $p_{e,z} = -1$ for $E' = 0$, $p_{e,z} = 0$ for $E' = E_c^0$, $p_{e,z} = E\sqrt{(1 - \cos \theta)}/2 = E \sin \theta/2$ for $E' = E$, and $p_{e,z} = 1 + E(1 - \cos \theta)$ for $E' = \infty$. Hence, $p_{e,z}$ varies over the interval $[-1, 1 + E(1 - \cos \theta)]$ as E' varies from 0 to ∞ .

2. The IA DDCS

The derivation of the IA-DDCS involves two steps. First Quantum Electrodynamics (QED) is used to obtain the DDCS for the scattering of the photon, characterized by 4 momentum (\vec{p}, E) , on a free and moving electron, of specified momentum and energy (\vec{p}_e^0, E_e^0) [8,16]. In the second step, the Compton effect is extended to the scattering of photons by the electrons in motion about the atom. The derivation assumes that electrons bound to an atom are simply free electrons with the momentum distribution characteristic of the atom. In a detailed quantum mechanical treatment the motion of bound electrons is restricted by the binding potential and by the rules of transitions. But in IA the bound moving electron DDCS is approximated [10,18,19] by the product of the free-electron DDCS and the atomic electron momentum distribution $\rho(\vec{p}_e)$, which is the Fourier transform of the square of the absolute value of the position wave function, for each shell i . The QM cross section calculation assumes that the Compton photon-electron interaction happens quickly (impulsively) such that the electron does not move significantly during the interaction and the potential felt by the electron during the interaction is constant. This allows the cross section to be computed from unperturbed wave functions. The removal of the electron from the atom requires that the momentum transfer is large. Hence, from the QM point of view, the validity of the IA approximation is conditioned by a quick and large momentum transfer.

Assuming an isotropic $\rho(\vec{p}_e)$ distribution the following IA DDCS result can be derived [8, 20, 21] for the i -th shell containing Z_i electrons,

$$\left[\frac{d^2\sigma}{dE' d \cos \theta} \right]_i = \pi r_0^2 \frac{E'}{E} \frac{1}{\sqrt{1+p_{\min}^2}} X(R, R') \cdot Z_i \frac{J_i(p_{\min})}{\Delta p}, \quad (5a)$$

where $R = E(\sqrt{1+p_{\min}^2} + (E-E')p_{\min}/\Delta p)$, $R' = R - EE'(1 - \cos \theta)$,

$$X = X(R, R') = \frac{R}{R'} + \frac{R'}{R} + 2 \left(\frac{1}{R} - \frac{1}{R'} \right) + \left(\frac{1}{R} - \frac{1}{R'} \right)^2, \quad (5b)$$

$$J_i(p_{\min}) = \int_{-\infty}^{\infty} dp_{e,x} \int_{-\infty}^{\infty} dp_{e,y} \rho(\sqrt{p_{e,x}^2 + p_{e,y}^2 + p_{\min}^2}) = \int_0^{2\pi} d\varphi \int_0^{\infty} dp' \cdot p' \rho(\sqrt{p'^2 + p_{\min}^2}) = \quad (5c)$$

$$2\pi \int_{|p_{\min}|}^{\infty} dp \cdot p \rho(p) \equiv J_{i,0} (1 + 2J_{i,0} |p_{\min}|) \exp \left[\frac{1 - (1 + 2J_{i,0} |p_{\min}|)^2}{2} \right]$$

The variable p_{\min} is the minimum of $p = \sqrt{p_{e,x}^2 + p_{e,y}^2 + p_{e,z}^2}$ when $-\infty < p_{e,x} < \infty$ and $-\infty < p_{e,y} < \infty$. If $p_{e,z}$ is assumed to be independent of $p_{e,x}$ and $p_{e,y}$, then, $p_{\min} = p_{e,z}(E, \cos \theta, E')$ leading to Eq. (4a) or similar approximations. But if $p_{e,z}$ is dependent on $p_{e,x}$ and $p_{e,y}$, as we will see in the BIA section, we use $p_{\min} = p_{e,z}(E, \cos \theta, E', p_{e,x} = 0, p_{e,y} = 0)$ in Eqs. (5). The Compton profile, $J_i(p_{e,z})$, as parameterized [20] by Eq. (5c), depends only on the parameter $J_{i,0}$. Tabulated [22] $J_{i,0}$ values for all atomic shells are available based on the Hartree-Fock symmetric atomic model. The function $J_i(p_{e,z})$ has a peak of height $J_{i,0}$ at $p_{e,z} = 0$ and attains a value of $0.5 J_{i,0}$ at $p_{e,z} = p_{e,z}^{0.5} = 0.9216 / 2J_{i,0}$ and $|E_c - E'(p_{e,z}^{0.5}, \cos \theta)|$. The parameter $J_{i,0}$ varies over the range of 1 to 250 (in units of $1/mc$; $1/mc$ unit = $1/137$ of the \hbar / mc^2 unit used in tabulation [22]). Hence, the function $J_{i,0}$ and the DDCS have significant values only for low values of $p_{e,z}$. Notice also that

$$\int_{-\infty}^{\infty} dp_{e,z} J_i(p_{e,z}) = 1 \quad (6)$$

If only energy and momentum conservation of free electrons moving according to the probability distribution $\rho(p)$ are considered, then events with $E' > E$ are not excluded. In practical calculations it is assumed that (QM conditions) $E' < E - U_i$ and $E > U_i$.

With the above restrictions, the IA DDCS for a mixture of atoms with the atomic fraction, f_i , becomes [20, 21]

$$\frac{d^2\sigma}{dE' d \cos \theta} = \pi r_0^2 \frac{E'}{E} \frac{1}{\sqrt{1+p_{e,z}^2}} X \cdot \sum_i \Theta(E - E' - U_i) f_i Z_i \frac{J_i(p_{e,z}(E, \cos \theta, E'))}{\Delta p}, \quad (7)$$

where $\Theta(x)$ is the Heaviside function (0 if $x < 0$, 1 if $x \geq 0$), and $p_{e,z}(E')$ given by Eq. (4). The Θ function discontinuously reduces the i -th shell contribution to zero for E' larger than $E - U_i$, leading to the discontinuities shown in Figures. 2(a) and 2(b). Since we assume that $E' \geq 0$, the i -th shell contributes nothing to the total DDCS when $E < U_i$, and hence, the DDCS decreases to zero when the incident photon energy E falls below the smallest binding energy, $\min(U_i)$, of the mixture

Eq. (7) can be rewritten as

$$\frac{d^2\sigma}{dE'd\cos\theta} = \pi r_0^2 \left(\frac{E_c^0}{E}\right)^2 X_{KN} G(E, \cos\theta, E') J(p_{e,z}) = \frac{d\sigma_{KN}}{d\cos\theta} G(E, \cos\theta, E') J(p_{e,z}) \quad (8a)$$

where

$$\frac{d\sigma_{KN}}{d\cos\theta} = \pi r_0^2 \left(\frac{E_c^0}{E}\right)^2 X_{KN}, \quad X_{KN} = \frac{E_c^0}{E} + \frac{E}{E_c^0} - \sin^2\theta, \quad (8b)$$

$$G(E, \cos\theta, E') = \left(\frac{E}{E_c^0}\right)^2 \frac{E'}{E} \frac{1}{\sqrt{1+p_{e,z}^2}} \frac{X}{X_{KN}} \frac{1}{\Delta p}, \quad (8c)$$

$$J(p_{e,z}) = \sum_i \Theta(E - E' - U_i) f_i Z_i J_i(p_{e,z}(E, \cos\theta, E')).$$

The last expression is zero for all $E' > \max_i(E - U_i) = E - \min_i(U_i)$. It is also zero for all $E < \min_i(U_i)$.

Also, we can write

$$\frac{d^2\sigma}{dp_{e,z}d\cos\theta} = \frac{d\sigma_{KN}}{d\cos\theta} F(E, \cos\theta, p_{e,z}) J(p_{e,z}) \quad (9a)$$

where

$$F(E, \cos\theta, p_{e,z}) = G(E, \cos\theta, E') \frac{dE'}{dp_{e,z}} = \left(\frac{E'}{E_c}\right)^2 \frac{1}{\sqrt{1+p_{e,z}^2}} \frac{X}{X_{KN}} \frac{\Delta p(E_c)}{\Delta p}. \quad (9b)$$

The function F is unity at $p_{e,z} = 0$ (where $E' = E_c$ and $J(p_{e,z}) = J_{i,0} = \text{maximum}$). Significant deviation from unity occurs only when $J(p_{e,z})$ differs significantly from zero and can therefore be approximated [21] by a linear function around 1. This range is centered about zero and is usually, but not always, included in the interval $(-1, 1)$.

3. The Impulse Approximation SDCS

The energy integration of the i -th atomic shell contribution Eq. (5a), leads to

$$\left[\frac{d\sigma}{d\cos\theta} \right]_{IA} = \frac{d\sigma_{KN}}{d\cos\theta} S_{IA}(E, \theta, Z), \quad (10)$$

where

$$S_{IA}(E, \theta, Z) = \sum_i f_i Z_i \Theta(E - U_i) S_i(E, \cos\theta, U_i), \quad (10b)$$

$$S_i(E, \cos\theta, U_i) = \int_0^{E-U_i} dE' G(E, \cos\theta, E') J_i(p_{e,z}(E, \cos\theta, E')), \quad (10c)$$

or

$$S_i(E, \cos\theta, U_i) = \int_{-\infty}^{p_{e,z}^{i, \max}} dp_{e,z} F(E, p_{e,z}, \cos\theta) J_i(p_{e,z}) \quad (10d)$$

with

$$F(E, p_{e,z}, \cos \theta) = G(E, E'(p_{e,z}, \cos \theta), \cos \theta) * dE' / dp_{e,z} \quad (10e)$$

$$p_{e,z}^{i,\max} = p_{e,z}(E, E' = E - U_i, \cos \theta)$$

III. BLENDED IMPULSE APPROXIMATION

A. A more exact energy-momentum relation

An exact solution of the EMC Eqs. (3f) leads to the following expression for $p_{e,z}$,

$$p_{e,z}(E, \cos \theta, E', p_{e,x}^2, p_{e,y}^2) = \frac{\Delta p E E' (1 - \cos \theta) \pm \sqrt{(E E' (1 - \cos \theta))^2 + 2 E E' (1 - \cos \theta) (1 + p_{e,x}^2 + p_{e,y}^2)} |E - E'|}{2 E E' (1 - \cos \theta)} \quad (11a)$$

or,

$$E'(E, \cos \theta, p_{e,z}^2, p_{e,x}^2, p_{e,y}^2) = E \varepsilon \frac{\sqrt{1 + \bar{p}^2} + \varepsilon(1 + \bar{p}^2 - \sqrt{1 + \bar{p}^2}) - \varepsilon \cos \theta p_{e,z}^2 \pm \sqrt{D}}{[1 + \varepsilon(\sqrt{1 + \bar{p}^2} - 1)]^2 - \varepsilon^2 p_{e,z}^2}, \quad (11b)$$

where $\varepsilon = E^0/E$ and

$$D = \left[\sqrt{1 + \bar{p}^2} + \varepsilon(1 + \bar{p}^2 - \sqrt{1 + \bar{p}^2}) - \varepsilon \cos \theta p_{e,z}^2 \right]^2 - \left[[1 + \varepsilon(\sqrt{1 + \bar{p}^2} - 1)]^2 - \varepsilon^2 p_{e,z}^2 \right] (1 + p_{e,x}^2 + p_{e,y}^2). \quad (11c)$$

The double sign term in Eq. (11a) is zero at $E' = E$, and the minus and plus sign should be used below and above $E' = E$, respectively. The minus sign in Eq. (11b) is valid for $p_{e,z} < 0$, while the plus sign is valid for $p_{e,z} > 0$ (D is zero at $p_{e,z} = 0$). In contrast to Eqs. (4a) and (4b), $p_{e,z}$ and E' are no longer in a one-to-one relation, because $p_{e,x}$ and $p_{e,y}$ occur as free parameters. Figures 4(a) – 4(c) show the dependence of E' on $p_{e,z}$, as given by Eqs. (4) and (11b), assuming average values for $p_{e,x}^2$ and $p_{e,y}^2$.

To evaluate the integral J in the IA-DDCS (Eq. (5a)), we assumed Eq. (4a) where $p_{e,z}$ is independent of $p_{e,x}$ and $p_{e,y}$ and hence, $p_{\min} = p_{e,z}(E, \cos \theta, E')$. In contrast, when Eq. (11a) is used, then we use $p_{\min} = p_{e,z}(E, \cos \theta, E', p_{e,x}=0, p_{e,y}=0)$.

Figures 4(a)-4(c) show $\text{Log} E'$ is approximately linear in $p_{e,z} \in (-1, 1)$ for Eq. (11a), in contrast with the approximate case Eq. (4a). Secondly, the slope of energy-momentum dependence strongly decreases as the scattering angle approaches zero. Since Eqs. (11) are approximated by Eqs. (4) for small values of $p_{e,x}, p_{e,y}, p_{e,z}$, we can estimate the value of the constant slope $d \text{Log} E' / dp_{e,z}$ from Eqs. (4) for small $p_{e,z}$. We have:

$$\left[\frac{1}{E'} \frac{dE'}{dp_{e,z}} \right]_{p_{e,x}^2=p_{e,y}^2=0}^{\text{exact}} \cong \left[\frac{1}{E'} \frac{1}{dp_{e,z}} \right]_{p_{e,x}^2=p_{e,y}^2=0}^{\text{IA}} = \left[\frac{E_c^0 \Delta p(E') / E / E'}{[1 - p_{e,z} E_c^0 (E' - E \cos \theta) / (E \Delta p(E'))]} \right]_{p_{e,z}=0} = \frac{\Delta p(E_c)}{E}, \quad (11d)$$

where $E_c^0 = E'(p_{e,x}=p_{e,y}=p_{e,z}=0)$.

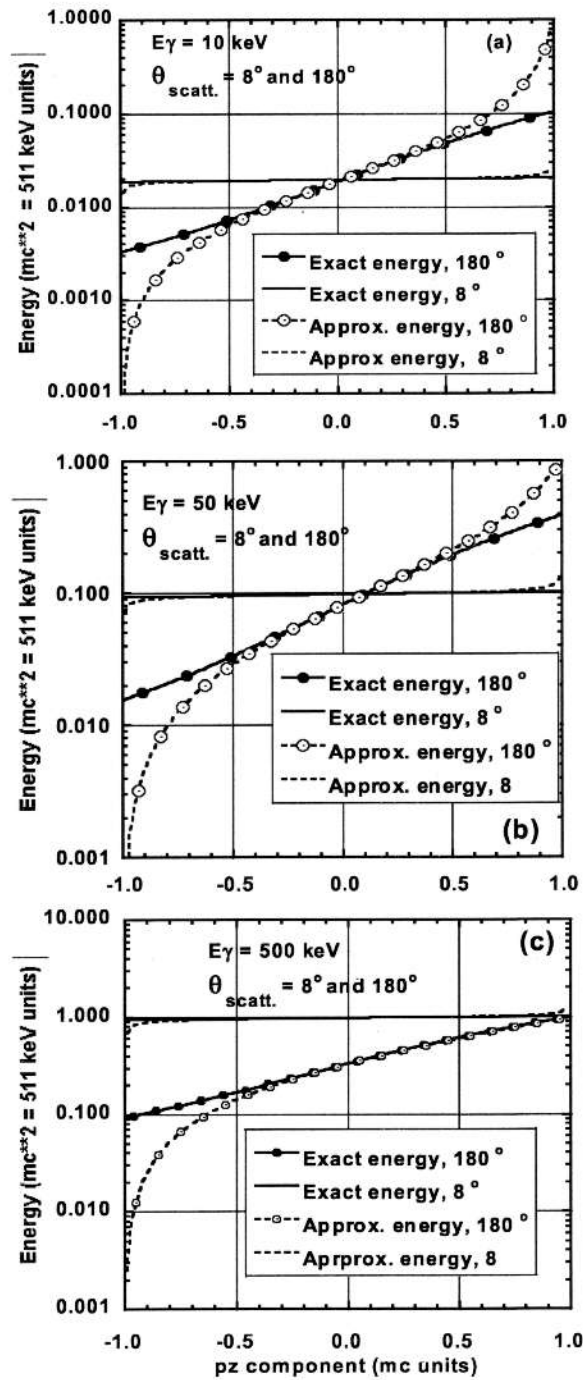


FIG. 4. Comparison of the exact and the approximate dependence of the emergent photon energy on $p_{e,z}$ at 8 and 180 degrees. a) 10 keV photons, b) 50 keV and c) 500 keV.

Finally, a few values of $p_{e,z}$ are as follows: $p_{e,z} = -\infty$ for $E' = 0$, $p_{e,z} = 0$ for $E' = E_c = E/(1 + E(1 - \cos \theta)/(1 + p_{e,x}^2 + p_{e,y}^2))$, $p_{e,z} = E\sqrt{(1 - \cos \theta)/2} = E \sin \theta / 2$ for $E' = E$, and $p_{e,z} = \infty$ for $E' = +\infty$. Hence, $p_{e,z}$ varies from $-\infty$ to $+\infty$ when E' varies from 0 to $+\infty$, a different behavior than in the standard implementation of IA.

B. The concept of electron partial (or rescaled) momentum

The main purpose of our paper is to propose an ad hoc modification to the relationship $E' = E'(p_{e,z})$ that eliminates the IA-DDCS sharp discontinuities and improves agreement with experiment in the vicinity of $E-U_i$. As in the IA, $p_{e,z}$ is used to parameterize $J_i(p_{e,z})$. But now we assume that only a part $p_{e,z}^{\text{eff}}$ of $p_{e,z}$, denoted by $p_{e,z}^{\text{eff}}$, can participate in the the momentum transfer between the electron and the photon. We seek a monotonic nonlinear transformation g : $p_{e,z} = g(p_{e,z}^{\text{eff}})$. We require g to restrict the energy $E'' = E'(p_{e,z}^{\text{eff}}, p_{e,x} = 0, p_{e,y} = 0)$, calculated by Eq. (11b), to the interval $[0, E]$. Thus g must confine $p_{e,z}^{\text{eff}}$ to the interval $(-\infty, E\sqrt{(1 - \cos \theta)/2})$. Therefore, acceptable rescaling functions, g , must satisfy

$g : (-\infty, E\sqrt{(1 - \cos \theta)/2}] \xrightarrow{\text{monotonic}} (-\infty, +\infty)$. In addition, the condition $g(0) = 0$ has to be satisfied if we wish to preserve the position of Compton peak maximum. But this condition is not strictly necessary. Also, a shell dependent $p_{e,z} = g(p_{e,z}^{\text{eff}})$ could be proven useful for a more detailed description of both total and shell DDCS. Here, our purpose is only to illustrate the method and hence, we use only $p_{e,z} = g(p_{e,z}^{\text{eff}})$ with $g(0) = 0$. To simplify the notation, we will write $p_{e,z}(p_{e,z}^{\text{eff}})$ instead of $g(p_{e,z}^{\text{eff}})$ and $p_{e,z}^{\text{eff}}(p_{e,z})$ instead of $g^{-1}(p_{e,z})$.

Application of a scaling function g subject to the above constraints is equivalent to limiting the target electron momentum that can participate in the collision to a fraction of that available. In the absence of a theoretical foundation for "partial electron momentum," g can be selected empirically. One simple implicit form of g with $g(0) = 0$, is:

$$p_{e,z} = p_{e,z}(p_{e,z}^{\text{eff}}) = p_{e,z}^{\text{eff}} / (1 - E'(p_{e,z}^{\text{eff}}) / E) + b, \quad (12a)$$

where $E'(p_{e,z}^{\text{eff}})$ is calculated from Eq. (11b). Two simpler explicit forms are

$$p_{e,z}(p_{e,z}^{\text{eff}}) = \left\{ \begin{array}{ll} a \cdot p_{e,z}^{\text{eff}} / (1 - p_{e,z}^{\text{eff}} / E\sqrt{(1 - \cos \theta)/2}) + b & \text{if } 0 \leq p_{e,z}^{\text{eff}} \leq E\sqrt{(1 - \cos \theta)/2} \\ p_{e,z}^{\text{eff}} + b & \text{if } p_{e,z}^{\text{eff}} < 0 \end{array} \right\}, \quad (12b)$$

$$p_{e,z}(p_{e,z}^{\text{eff}}) = \left\{ \begin{array}{ll} p_{e,z}^{\text{eff}} / (1 - \sqrt{p_{e,z}^{\text{eff}} / E\sqrt{(1 - \cos \theta)/2}}) + b & \text{if } 0 \leq p_{e,z}^{\text{eff}} \leq E\sqrt{(1 - \cos \theta)/2} \\ p_{e,z}^{\text{eff}} + b & \text{if } p_{e,z}^{\text{eff}} < 0 \end{array} \right\} \quad (12c)$$

where a and b are constants to be chosen. Eqs. (12b) and (12c) are easily invertible, a useful property for Monte Carlo simulations. With these definitions, $E'' = E'(p_{e,z}^{\text{eff}}, p_{e,x} = 0, p_{e,y} = 0) \in [0, E]$, while J_i from Eq. (5c) describing the electron momentum distribution in the atom, is still a function of $p_{e,z}$. Notice that $p_{e,z}(p_{e,z}^{\text{eff}} = 0) = 0$ if $b = 0$ and hence, the DDCS peak value occurs when either the actual or rescaled momentum is zero. We use here only the case of $b = 0$. However, through selection of the additive constant b , Eqs. (12) can be used to shift the Compton peak according to experimental data.

C. Blended Impulse Approximation

We combine the ISF and IA approximations to yield a DDCCS that can be adapted systematically to match experimental data, such that its integral over energy is equal to the ISF SDCS, or to an experimentally corrected ISF SDCS. Combining the incoherent-scattering function with a Compton profile has been used previously [9] to obtain a non-adaptable IA-DDCCS. Our approach allows independent adjustment of the DDCCS energy spectrum shape, via $p_{e,z}$ scaling, and the adjustment of the SDCS and total-cross-sections from an ISF database.

First, similar with IA, Eq. (8a), we can write

$$\begin{aligned} \left[\frac{d^2\sigma}{dE' d\cos\theta} \right]_{BIA} &= \frac{d\sigma_{ISF}}{d\cos\theta} \frac{G(E, \cos\theta, E') J(p_{e,z})}{S_{BIA}(E, \theta, Z)} \\ &= \frac{d\sigma_{ISF}}{d\cos\theta} \frac{G(E, \cos\theta, E') J(p_{e,z})}{\sum_i f_i Z_i S_i^\infty}, \end{aligned} \quad (13a)$$

where

$$\begin{aligned} S_i^\infty(E, \cos\theta) &= \int_0^\infty dE' G(E, \cos\theta, E') J_i(p_{e,z}(E, \cos\theta, E')) = \\ &= \int_{-\infty}^\infty dp_{e,z} F(E, \cos\theta, p_{e,z}) J_i(p_{e,z}) \\ J(p_{e,z}) &= \sum_i f_i Z_i J_i(p_{e,z}(E, \cos\theta, E')). \end{aligned} \quad (13b)$$

Note that no restrictions of the form $E' < E - E_i$ and $E - E_i > 0$ are placed on the limits of integration. Integrating over E' for fixed θ , yields exactly the ISF SDCS. S_i^∞ is very close to unity for all shells except the tightly bound (K) shells. Notice that the above procedure can also be applied to shell ISF data if available. In this case, Eq. (13a) becomes

$$\left[\frac{d^2\sigma}{dE' d\cos\theta} \right]_{BIA} = \sum_i \left[\frac{d\sigma_{ISF}}{d\cos\theta} \right]_{shell\ i} \frac{G(E, \cos\theta, E') f_i Z_i J_i(p_{e,z})}{\sum_i f_i Z_i S_i^\infty}. \quad (13c)$$

Eq. (13a) will allow scattered photons to exceed E , as shown by Fig. 2(a). An ad hoc form of the DDCCS, one that retains the Compton profile maximum position and follows the trend of the experimental values, is obtained by using partial electron momentum rescaling to map Eq. (13a) from the interval $E' \in [0, \infty)$ into the interval $E'' \in [0, E]$, and by rescaling it with the adequate multiplication constant to give the proper E'' integral, i.e., the ISF SDCS.

Using $p_{e,z}^{eff} = e(E'')$ and $p_{e,z} = e(E')$ for Eq. (11a) and $p_{e,z} = g(p_{e,z}^{eff}) = g(e(E''))$ for Eqs. (12a) to (12c) then $e(E') = g(e(E''))$ or $E' = e^{-1}(g(e(E'')))$ and $E'' = e^{-1}(g^{-1}(e(E')))$. The desired DDCCS in the energy E'' is then defined as

$$\left[\frac{d^2\sigma}{dE'' d\cos\theta} \right]_{BIA} = \frac{d\sigma_{ISF}}{d\cos\theta} C(E, \cos\theta) \frac{G(E, \cos\theta, E'(E'')) J(p_{e,z}(p_{e,z}^{eff}(E'')))}{\alpha(E, \cos\theta)} \quad \text{if } E_c < E'' \leq E \quad (14a)$$

$$\left[\frac{d^2\sigma}{dE' d\cos\theta} \right]_{BIA} = \frac{d\sigma_{ISF}}{d\cos\theta} C(E, \cos\theta) \frac{G(E, \cos\theta, E') J(p_{e,z}(E'))}{\alpha(E, \cos\theta)}, \quad \text{if } 0 \leq E'' = E' \leq E_c. \quad (14b)$$

Here,

$$\alpha(E, \cos\theta) = \int_0^E dE'' G(E, \cos\theta, E''(E'')) J(p_{e,z}(p_{e,z}^{eff}(E''))) \quad (14c)$$

We included with Eqs. (14a) and (14b) a multiplicative correction factor $C(E, \cos(\theta))$, whose values are unity unless we can evaluate from experiment better values, to increase its adaptability to the experimental values..

Since Eq. (14c) contains the whole atom ISF function, the values of C derived from experiment are likely to be close to unity in most of the cases, in view of the comparisons of the whole atom ISF results with the experiments [17]. If ISF data are available for individual shells, Eq. (14c) can be appropriately changed, similarly to eq (13c). In this case, the correction factor is split into individual shell correction factors, which could be significantly different from unity for lower shells.

Figures 5(a) and 5(b) compare BIA (Eqs. (14), (12b) with $a = 2$), IA, and S-matrix calculations to experimental results to show the feasibility of the DDCS improvement by using momentum rescaling. The Gold K-shell BIA-SDCS of Fig. 5(a) was scaled (as suggested above) by setting $C = 1.667$ to better fit the experimental data. It shows that the BIA-DDCS shape differs essentially from IA and S-matrix and that it follows the decrease shown by the experiment in the vicinity of $E - U_K$. For scattering of 70 keV photons by Cu, BIA also removes the sharp decrease in the DDCS, Fig. 5(b). From this figure it can be seen that while BIA inherently does not allow photon energies larger than the incident photon energy, it does allow Compton scattered photons of energy higher than $E - U_K$. The $p_{e,z} - p_{e,z}^{eff}$ relationship, Eq. (12c), leads to similar results for Gold. Hence, an appropriate ad hoc fraction of the electron momentum can improve dramatically the DDCS. If studied systematically for different shells and atoms, this procedure might also lead to physical consequences for the photon or for its scattering mechanism.

For Tin, we found that the BIA-DDCS derived from Eq. (12c) decreases faster than the experimental curve shown in Fig. 1(b) in the vicinity of $E - U_K$, indicating that a more appropriate $p_{e,z} - p_{e,z}^{eff}$ relationship is needed for this case. Clearly the BIA model can accommodate this task by a selection of shell dependent-constant C and of the scaling function $g(p_{e,z}^{eff})$, to match the experimental DDCSs.

However, meaningful work in this direction requires a consistent set of sufficiently accurate experimental DDCSs, for a range of incident photon energies.

Fig. 5(c) compares the total (all-shell) BIA-DDCS, using Eqs. (14) and $p_{e,z} = g(p_{e,z}^{eff})$ of Eq. (12b) with $a = 4$, to the energy-restricted total IA-DDCS for photons of 10 keV scattered by Cu. In contrast to IA-DDCS, the BIA-DDCS has no discontinuities and goes smoothly to zero in the vicinity of the incident photon energy. Again, such a difference must be tested experimentally in detail, and depending on the results, this will help choosing a shell-dependent or a shell-independent $p_{e,z} = g(p_{e,z}^{eff})$.

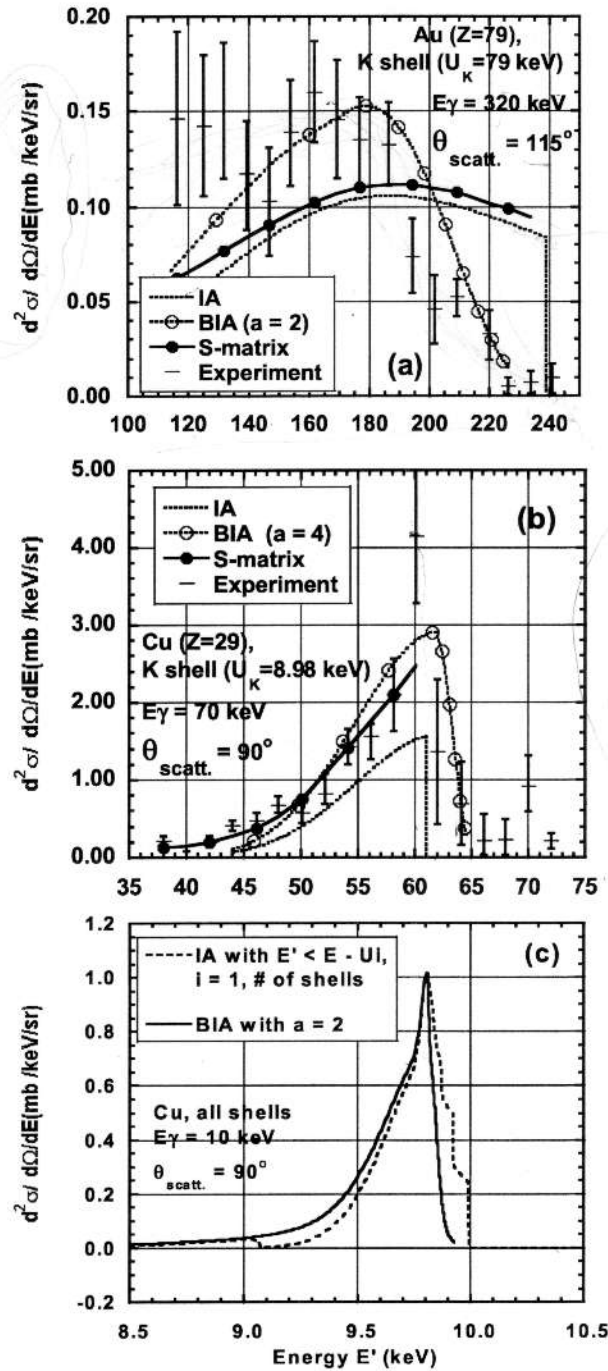


FIG. 5. a) Comparison of BIA-DDCS ($a = 4$) with IA, S-matrix and experimental data, $E = 320$ keV photons scattered on the K-shell of Au at 115 degrees. b) Comparison of BIA-DDCS ($a = 4$) with the IA-DDCS and experiment, $E = 70$ keV scattered on the K-shell of Cu at 90 degrees. c) Comparison of the BIA-DDCS ($a = 2$) and the IA-DDCS, for an incident energy $E = 10$ keV scattered on Cu (all shells) at scattering angle of 90 degrees.

IV. CONCLUSIONS

A review of the Impulse Approximation (IA) for calculating Compton photon-electron scattering probabilities reveals a paucity of measured, double-differential cross-section (DDCS) data with respect to angle and energy, especially for scattered photons in the energy region near the incident photon energy E . The K-shell DDCSs derived from IA display undesirable discontinuities and poorly match available experimental continuous DDCSs between the Compton energy E_c^0 and E . Similar discrepancies with respect to experiment are displayed by the S-matrix results. Because numerical evaluation of IA is so straightforward, we have proposed an ad hoc modification, called the blended impulse approximation (BIA) that combines the incoherent scattering approximation, an IA-like approximation for the DDCS, and an ad hoc concept of partial (rescaled) electron momentum that replaces the electron momentum in the energy-momentum conservation relations. The empirical relationship between the rescaled (partial) momentum and original target electron momentum, can be manipulated to improve the agreement between predicted and measured DDCSs, and to eliminate unphysical discontinuities.

The BIA method results in a DDCS that has a number of advantages. BIA removes the undesirable discontinuities in the DDCS, indicates better agreement with existing experimental data, and provides a general DDCS form for incorporating evaluated experimental data. Its energy integral exactly reproduces the SDCS obtained by correcting the Klein-Nishina distribution by the ISF factor. A multiplicative constant, assumed to be unity in the absence of experimental data, can be used to improve the ISF approximation. This constant can be manipulated to improve the fit to experimental data when available. Further improvement requires finding an optimal partial electron momentum function, and the evaluation of an ISF scaling factor as experimental data becomes available. A comprehensive DDCS measurement for the Compton effect on bound electrons is necessary for finding an optimal partial electron momentum function. The ad hoc BIA-DDCS method that uses a parameter-free partial momentum transformation, can be readily used in Monte Carlo photon transport codes. Therefore, the BIA procedure and the electron momentum rescaling provide, at this stage, an empirical tool for systematically improving agreement with the experimental data for the DDCS and the SDCS, in photon scattering on bound electrons.

Finally, we suggest two more powerful resources associated with the concept of partial electron momentum. a) Since S-matrix DDCS's display similar behavior as the IA-DDCS in the vicinity of $E-U_K$, the ad hoc concept of partial electron momentum could also be used in the context of S-matrix with similar benefits. b) The partial electron momentum might have a direct physical significance for the photon: the Compton interaction is such that the photon sees only a part of the electron momentum. If further considerations do not allow such a direct physical significance, then the partial electron momentum might indicate the need for a revised mechanism of the Compton effect, different for free and bound electrons. The experiment of looking for electron-electron correlations in the Compton effect might be a starting point toward a revised mechanism.

Acknowledgements

The present work was supported by grant R01 CA 46640 awarded by NIH. C. I. Costescu expresses his gratitude to Dr. Larry W. Burggraf for support during a previous review of the IA DDCSs.

-
- [1] A.H. Compton, Phys. Rev. **21**, 483 (1923). A.H. Compton, Phys. Rev. **22**, 409 (1923).
- [2] A.H. Compton, S.K. Allison, *X-rays in Theory and Experiment* (D. Van Nostrand Company, NY, 1935).
- [3] J.H. Hubbell, Wm.J. Veigle, E.A. Briggs et al., Phys. Chem. Ref. Data **4**, 471 (1975).
- [4] *Compton Scattering*, edited by B. Williams (McGraw Hill, Inc., Printed in Great Britain, 1977).
- [5] T.Aberg, J Tulkki, in *Atomic Inner-Shell Physics*, Edited by B. Crasemann (Plenum, New York, 1985), p. 419.
- [6] P.M. Bergstrom Jr., R.H. Pratt, Radiat. Phys. Chem. **50**, 3 (1997).
- [7] R.W. James, *The optical principles of the diffraction of x-rays* (Ox Bow Press, Woodbridge-Connecticut, 1982), (originally published by G. Bell and Sons, London, in 1946).
- [8] R. Ribberfors and K.F. Berggren, Phys. Rev. A **26**, 3325 (1982). R. Ribberfors, Phys. Rev. B **12**, 2067 (1975).
- [9] Y. Namito, S. Ban, H. Hirayama, Nucl. Instr. and Meth. in Phys. Res. A **349**, 489 (1994).
- [10] P.M. Bergstrom, T. Suric, K. Pisk, R.H. Pratt, Phys. Rev. A **48**, 1134 (1993).
- [11] S.M. Lad, G. Basavaraju, P.P. Kane, Phys. Rev. A **42**, 1267 (1990).
- [12] G. Basavaraju P.P. Kane, S.M. George, Phys. Rev. A **36**, 655 (1987).
- [13] V. Marchetti, C. Franck, Phys. Rev. A **39**, 647 (1989).
- [14] A. Reineking, R. Wenskus, A. Baumann et al., Phys. Lett. **95A**, 29 (1983)
- [15] W. Heitler, *The Quantum Theory of Radiation* (Oxford Univ. Press, Printed in Great Britain, 1954).
- [16] J.M. Jauch and F. Rohrlich, *The theory of Photons and Electrons* (Springer, Berlin, 1976).
- [17] J.H. Hubbell, Radiat. Phys. Chem. **50**, 113 (1997).
- [18] P. Platzman and N. Tzoar, in *Compton Scattering*, Edited by B. Williams (McGraw-Hill, Inc., 1977) pg. 28.
- [19] P. Eisenberger and P.M. Platzman, Phys. Rev. A **2**, 415 (1979).
- [20] D. Brusa, G. Stutz, J.A. Reveros, J.M. Fernandez-Varea, F. Salvat, Nucl. Instrum. and Methods in Phys. Res. A **379**, 167 (1996).
- [21] I. Kawrakow and D.W.O. Rogers, NRCC Report PIRS-701, April 20, 2000.
- [22] F. Biggs, L. Mendelsohn, and J. Mann, At. Data and Nucl. Data Tables **16**, 201 (1975).